According to the project proposal, the following objectives have been investigated and solved in stage III/2014 of the project:

O1/ Identification of parameters that affect the physico-chemical properties of non-noble bimetallic nanoparticles (Cu and Co) supported on SBA-15.

A1.1. Preparation of CuCo/SBA-15 materials by MDI method.

A1.2. Preparation of CuCo/SBA-15 with various ratios M_1:M_2.

At this stage, considering the results of phase II/2013, the studies have been extended towards the deposition of bimetallic nanoparticles (Cu and Co) on mesoporous silica of SBA-15 type with optimized textural properties (in the stage I/2012 studies on the size of primary mesopores and the ratio between micro- and primary mesopores have been done). SBA-15 used as support was calcined and stored under controlled conditions of moisture up to the preparation of catalytic materials by MDI method[1]. Because the studies concerning CuNi system have pointed out a degree of 5% loading with metal as optimum, at this stage, our studies have been mainly directed on the mono-metallic materials Cu/ SBA-15 and Co/SBA-15 (*activity A1.1*) and on the effect of the mass ratio M_1:M_2 (M_1 = copper, M_2 = cobalt; M_1:M_2 = 8:2, 5:5, 2:8) - at constant loading degree of 5% metal (*activity A1.2*) - on the physico-chemical and catalytic properties of bimetallic system CuCo/SBA-15. Within the *activity 1*, a sample of Co/SBA-15 with 10% loading was also prepared and used as reference for comparison with a set of mono-metallic catalysts prepared by melt infiltration method. For the synthesis of these materials, copper and cobalt nitrates were used as metal precursors. The obtained samples were dried at 25 ° C for 48 h and then calcined at 500°C (ramp of 1.5 °C/min, 6 h at the final temperature).

O2/ Advanced characterization of CuCo/SBA-15 materials.

A2.1. Characterization of CuCo/SBA-15 materials in relation to their structural and textural properties

A2.2. Cheracterization of bulk and surface chemical composition of CuCo/SBA-15 materials.

A2.3. Characterization of reducibility, thermostability and the nature of catalytic active sites of CuCo/SBA-15 materials.

After calcination, CuCo/ SBA-15 materials obtained by MDI were systematically analyzed by various techniques such as ICP-OES, DRX (large and small angles), nitrogen physisorption, (HR)TEM, TPR. Metallic forms were investigated by *in-situ* DRX after thermo-programmed reduction, (HR)TEM/EDX and chemisorption of N_2O.

The selection of the most significant results which are directly correlated with the proposed activities

The data obtained from the chemical analysis, nitrogen physisorption and DRX at large and small angles are presented in Table 1. It can be noted that the mass percentages experimentally evaluated for the samples of CuCo/SBA-15 type are close to those calculated both in terms of theoretical quantity of metal reported to support and mass ratios between the two metals.

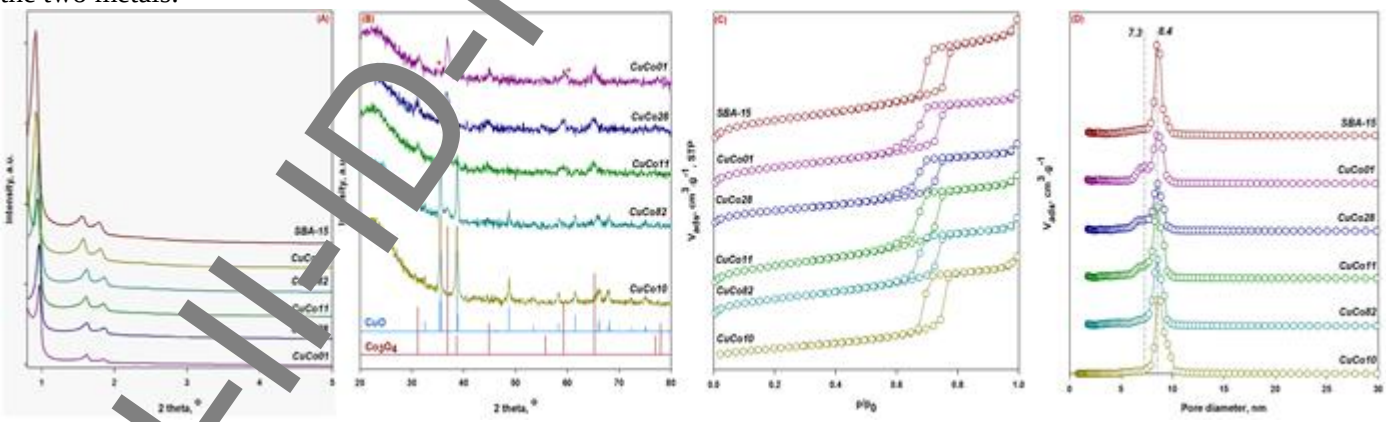

Fig. 1. XRD patterns at small (A) and high (B) angles for the calcined samples of CuCo/SBA-15 type. Nitrogen adsorption-desorption isotherms (C), and pore size distribution calculated by NL-DFT (E) for the calcined samples of CuCo/SBA-15 type.

Taking into account the X-rays diffraction data obtained at small angles and the results of nitrogen physisorption (Fig. 1A, C, and D) for SBA-15 support and mono-and two-component materials it can be affirmed that both SBA-15 support and materials containing copper and cobalt oxides present ordered mesostructures with cylindrical and parallel pores. As concerns the samples with monometallic copper (CuCo10), the results obtained in this study confirm those reported in stage II/2013 on a similar sample, namely, copper species present a high mobility that makes them difficult to be stabilized on a silica type support because of the weak interactions between copper precursors and support

surface. This effect is very well illustrated by XRD data at small angles (Fig. 1A and Table 1) and large angles (Fig. 1B) that indicate the presence of large copper oxide crystallites with a size of around 30 nm, located mainly on the external surface of SBA-15 granules.

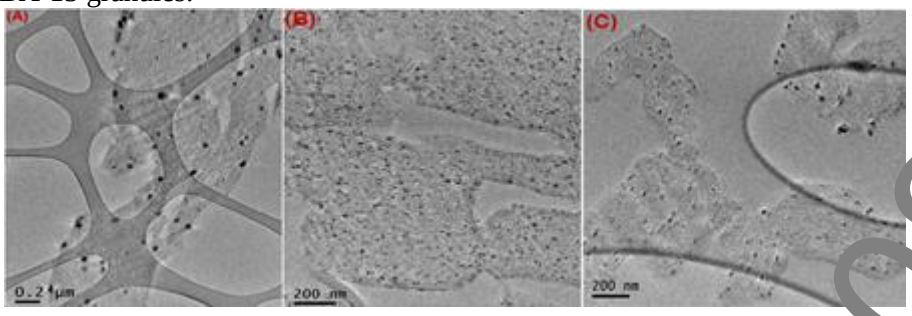

Fig. 2 Representative TEM images of calcined samples of CuCo/SBA-15 type: A – CuCo01, B – CuCo28, C – CuCo11

For the mono-metallic cobalt sample (CuCo01), one can notice a better stabilization of cobalt oxide particles within the mesopores of SBA-15. Indeed, the corresponding TEM image (fig. 2A) shows a distribution of polycrystalline cobalt oxide particles as nanorods inside the pores, associated in relatively large patches (fig. 3A), thus confirming the previous results of phase I/2012. This result could be explained by two effects as follows: (i) the first effect consists of the stabilization of Co_3O_4 nanoparticles in primary mesopores through the phenomenon of confinement (size of Co_3O_4 crystallites are very close to that of the average size of SBA-15 channels - Table 1); (ii) the second effect originates from the chemical interaction between the cobalt precursor and silica surface with formation of (phyllo)silicate type phases, most likely stevensite $Co_3(Si_2O_5)_2(OH)_2$[2]. It is interesting to note that the introduction of small amounts of copper besides cobalt (CuCo28) leads to an improvement of the dispersion of oxide particles in the mesostructured support (fig. 2B), while an equal ratio between the two elements (CuCo11) generates an intermediate situation between that described for mono-metallic cobalt sample and those for the sample with a ratio Cu:Co of 2:8. Actually, this result indicates two different effects: on the one hand, the effect of cobalt on the stabilization of copper phases on the silica support, and on the other hand the effect of copper on the dispersion of cobalt.

Table 1. Structural and textural properties of the SBA-15 support and calcined CuCo/SBA-15 materials

Sample	ICP		small angles XRD		N_2 physisorption					high angles XRD	
	Cu wt. %	Co wt. %	d_{100}[a] (nm)	a_0[b] (nm)	S_{BET}[c] ($m^2.g^{-1}$)	S_μ[d] ($m^2.g^{-1}$)	V_p[f] ($cm^3.g^{-1}$)	V_μ[e] ($cm^3.g^{-1}$)	Dp[g] (nm)	D_{CuO}[h] (nm)	D_{Co3O4}[h] (nm)
SBA-15	-	-	9.7	11.2	720	206	1.12	0.095	8.4	-	-
CuCo01	-	5.11	9.8	11.3	612	84	0.96	0.043	7.3; 8.4	-	9.3
CuCo28	1.32	4.67	9.2	10.6	760	114	1.10	0.042	7.3; 8.4	-	9.0
CuCo55	3.27	2.76	9.4	10.8	631	101	1.08	0.046	7.3; 8.4	-	8.1
CuCo82	5.44	1.19	9.3	10.7	575	99	1.09	0.041	8.4	29.2	6.9
CuCo10	4.41	-	9.7	11.2	663	59	0.8	0.027	8.4	32.0	-

[a]d_{100} interplanar distance; [b]$a_0 = 2d_{100}/\sqrt{3}$. [c]S_{BET} = specific surface area evaluated by BET equation ($P/P_0 = 0.1–0.25$). [d]S_μ and [e]V_μ = micropores surface and volume from *t*-plot; [f]V_{total} = pores volume determined at $P/P_0 = 0.97$; Dp = pores diameter by NL-DFT method for cylindrical pores; [h] crystallite size by Scherrer equation: $d_{hkl} = K(\lambda/\beta)\cos\theta$.

Furthermore, TPR data (Fig. 3A) clearly show a synergistic effect between these two elements, as also observed in the case of previously studied CuNi system[3]. Thus, if for mono-metallic samples relatively high reduction temperatures were observed (345 and 500 °C for CuCo10; 340-750 °C for CuCo01), for the bimetallic samples it can be seen a main reduction peak, located at ~ 300 °C, which is attributed to the simultaneous reduction of copper and cobalt cations from sample. In the case of CuCo10 sample, the two reduction temperatures are assigned to the reduction of Cu^{2+} to Cu^0 in bulk CuO poorly dispersed, and the second one (which is minor) is attributed to the reduction of Cu^{2+} from silicates or from CuO confined in micropores[3]. As concerns the cobalt sample, there are more reduction temperatures indicating (i) the presence of at least two species of cobalt in different interactions with silica and (ii) a heterogeneity of particle size of Co_3O_4.[2]

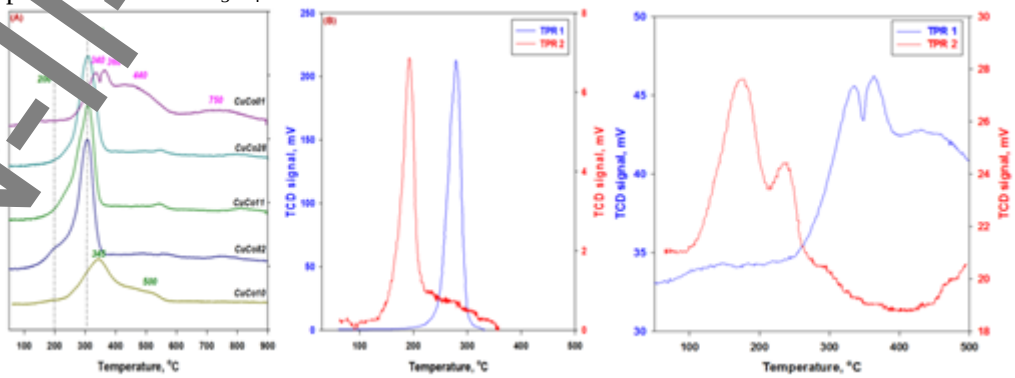

Fig. 3 TPR curves for samples of CuCo/SBA-15 type (A). TPR curves associated with N_2O chemisorption:
blue – TPR 1 – registered prior to titration with N_2O; **red – TPR 2** – TPR recorded after titration with N_2O; CuCo10 – (B) and CuCo01 – (C).

The evolution of crystalline phases and their thermostability during the reduction was monitored *in-situ* by DRX (Fig. 4). It can be seen that, in agreement with the chemical composition of the samples, the diffractograms contain peaks assigned to different crystalline phases. For example, for the mono-metallic cobalt sample, one observes the presence of Co_3O_4 in diffractograms recorded after reduction up to 350 °C, then the formation of CoO phase whose traces could be observed even after reduction at 450 °C. After reduction at 550 °C, it can be detected an extremely small diffraction peak at ~75 °, which is specific to metallic cobalt phase. Its intensity increases slightly with the reduction temperature, however, it is too small to apply the Scherrer equation. It is interesting to note that the XRD patterns recorded after reduction of CuCo28 up to 350 °C do not show any diffraction peak, indicating a very good dispersion of crystalline phases, in well agreement with the TEM images showing a maximum dispersion. Moreover, any peaks corresponding to metallic cobalt cannot be identified in XRD patterns, indicating their high dispersion. It can be also assumed the formation of heterostructures that shares an interface in which the two mixed metals are found in the synergistic interactions. A ratio of 1: 1 between the two elements (CuCo11) leads to a slight increase in the amount of copper that is not involved in the synergistic interaction, which is confirmed by the presence of diffraction peak corresponding to the plan (200) of metallic copper (2θ ~ 50.2 °). Thus, it can be seen that the peak corresponding to the phase of Cu^0 is identified starting with the reduction at 350 °C and it is relatively well-defined, but its intensity is relatively constant throughout the range of reduction from 350 °C up to 750 °C, indicating a stabilization of copper in the SBA-15 support. Diffractograms recorded for sample (CuCo82) contain specific diffraction peaks for both metallic phases, Cu^0 and Co^0, which would suggest the formation of nanoparticles of mono-metallic copper and cobalt. However, taking into account the TPR data, which display a reduction peak at ~ 200 ° C, likely due to the reduction of copper cations from nanoparticles of CuO-component, it can be asserted that in this sample would co-exist bimetallic heterostructures, where the two elements are in the synergistic interaction, and mono-metallic nanoparticles.

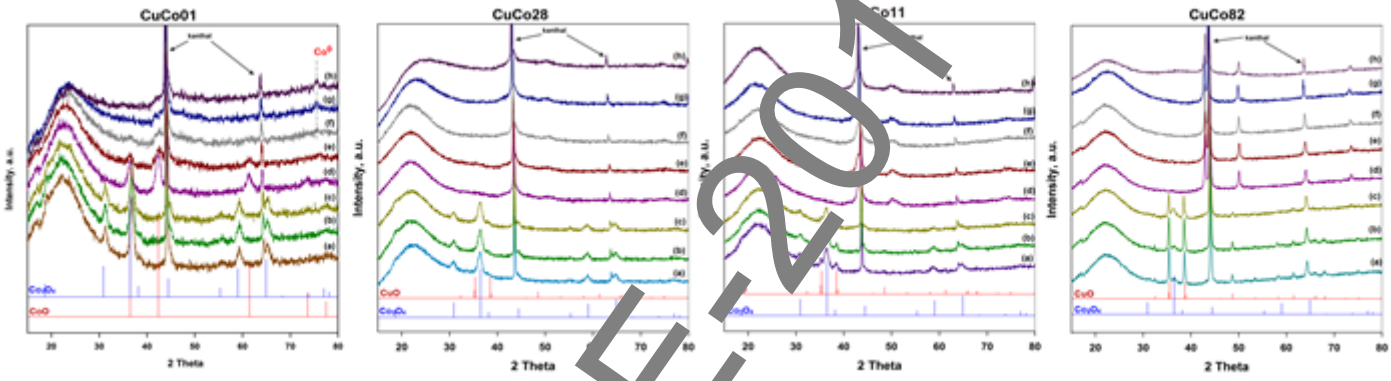

Fig. 4. XRD patterns recorded *in-situ* for the CuCo/SBA-15 samples after thermo-programmed reduction at 30 °C (a), 150 °C (b), 250 °C (c), 350 °C (d), 450 °C, (e) 550 °C (f), 650 (g) and 750 (e); (h) recorded after cooling under hydrogen at 30 °C.

The TEM images taken after reduction at 750 °C for CuCo01, CuCo28 and CuCo11 samples confirm all the above results. Thus, for CuCo01 sample (Fig. 5A), there are two types of particles, namely: (i) cobalt particles joined

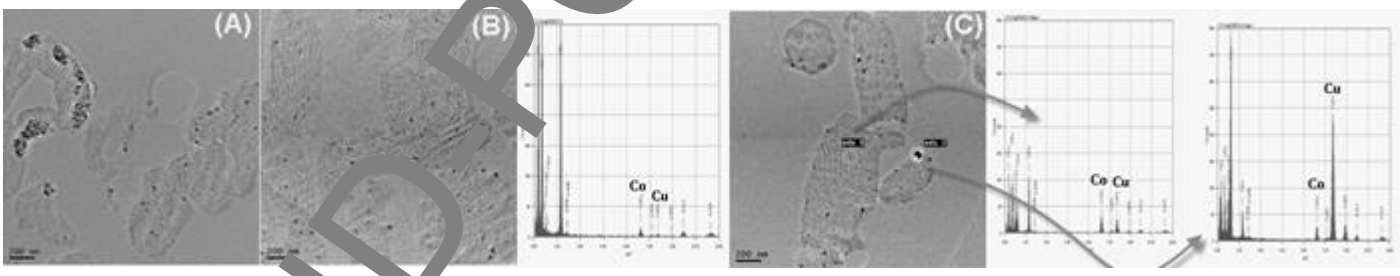

Fig. 5 Representative TEM images for catalysts of CuCo/SBA-15 type: A – CuCo01, B – CuCo28, C – CuCo11.

together in large agglomerates, but located inside the mesopores – this is possible due to the particular structure of SBA-15 silica in which primary mesopores are interconnected through secondary mesopores and micropores located in the wall of silica and (ii) cobalt particles very well dispersed in the mesopores of support.[2] For CuCo28 and CuCo11 one observes that the dispersion of metal nanoparticles is similar in both cases. Interestingly, EDX analysis shows different compositions for these nanoparticles. Thus, for the CuCo28, EDX analysis indicates the presence of the two metals in the same nanoparticle, with the mass ratio close to the theoretical one, thus supporting the hypothesis of heterostructures formation, while nanoparticles from CuCo11 sample although they contain both metals, they show either ratios close to the theoretical one or copper-rich compositions, in particular in the case of nanoparticles located on the external surface. However, cumulating the TPR and TEM results, it is evident that these extra-porous nanoparticles constitute a minor population.

Because these materials are designed to be used in the hydrogenation of cinnamaldehyde, we directed our studies on the evaluation of the catalytic active metal surfaces. According to the literature, in the case of copper, this is possible by titration with N_2O, the method being specific for this metal.[4-6] In practice, the method consists in the following. After a first step of thermo-programmed reduction of Cu^{2+} to Cu^0, a stream of N_2O is passed over the sample, when

the partial re-oxidation of the accessible copper atoms to Cu^+ takes place, and in the second-step, Cu^+ species are again thermo-programmed reduced to Cu^0. The dispersion of metallic copper was calculated from the areas measured for the two reduction peaks. Also, considering different parameters, the average diameter of the copper particles as well as the exposed surface of metallic copper can be calculated. TPR curves corresponding to sample CuCo10 are shown in Fig. 3B. It was evaluated a dispersion of 5.4% for metallic copper, with an active area of 3.7 $m^2 \cdot g_{catal}^{-1}$ and particles size of 18.4 nm. These results were predictable, but the analysis was conducted in order to have a comparison for bimetallic samples. Surprisingly, for bimetallic samples, the peaks areas obtained in the second-step reduction (TPR 2) were high, by taking into account the effective amount of copper. Consequently, an influence of the cobalt atoms could be suspected, yet this is not described in the literature. Therefore, it was carried out a new analysis for the sample CuCo01 (Fig. 3C). As it can be seen, both TPR curves (TPR 1 and TPR 2) show two maximum reduction temperatures. For TPR 1curve, they correspond to the two-step reduction of Co_3O_4 to Co^0 ($Co_3O_4 \rightarrow CoO \rightarrow Co^0$). After titration with N_2O, Co^0 is partially re-oxidized to CoO. It is known that the most stable form of cobalt oxide is Co_3O_4 and as a result, perhaps as a part from this CoO has been totally oxidized, which can explain the existence of the two maxima of reduction in the TPR 2 curve. In this case, the peaks are better defined and sharper and they result from the reduction of Co^{3+} and Co^{2+} to Co^0. These results highlight the non-specificity of method for copper when it belongs to bimetallic samples and data obtained for the other CuCo bimetallics are not reported.

O3/ Evaluation of catalytic properties of materials for the hydrogenation of cinnamaldehyde.

A3.1. Hydrogenation of cinnamaldehyde in the presence of catalysts based on CuCo at atmospheric pressure.

A3.2. Hydrogenation of cinnamaldehyde in the presence of catalysts based on CuCo under high pressures.

The catalytic materials developed in this phase of the project have been tested in the reaction of the liquid phase hydrogenation of cinamaldehidei using two sets of reaction conditions: (i) atmospheric pressure and 150 °C and (ii) 10 bar and 130 °C. The results illustrate the influence of reaction conditions and on the other hand, the influence of the mass ratio of the two metals and metallic particle size on the performance of catalytic materials.

(i) Results obtained for catalytic runs performed at atmospheric pressure and 150 °C

Conversion and selectivity curves obtained for catalytic tests carried out at atmospheric pressure are given in Fig. 6. It can be seen that the catalytic activity of mono-metallic copper-based materials is virtually zero, which is in agreement with data of XRD, TPR and chemisorption of N_2O. For this reason, the results about selectivity obtained on this catalyst are not relevant and are not presented here.

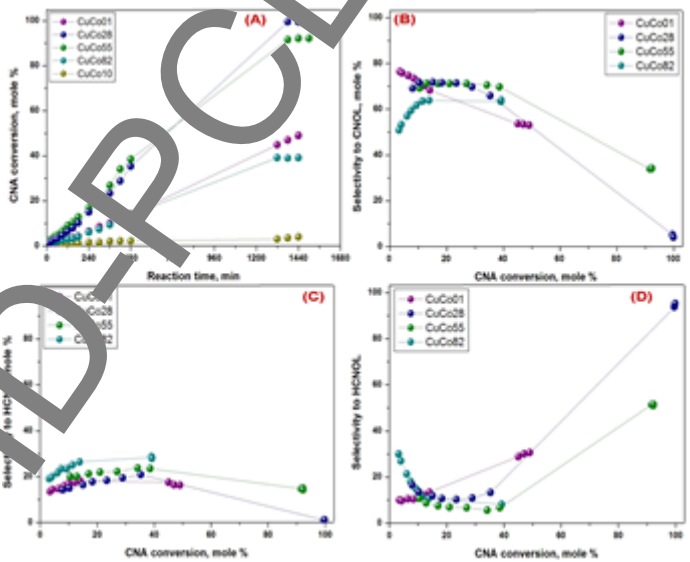

Fig. 6 Conversion of CNA vs. reaction time (A), selectivity to CNOL (B), HCNA (C) and HCNOL (D) for CuCo/SBA-15 catalysts. (Reaction conditions: *T_{red} = 500 °C for sample CuCo01 and 350 °C for the others; $T_{reaction}$ = 150 °C, 0.265 g catalyst; 1 mL CNA, 25 mL propylene carbonate as solvent, flow rate of H_2 = 1 L h^{-1}, speed of agitation = 900 rpm*).

The gradual introduction of a quantity of cobalt to copper lead to an improvement in activity so that a maximum conversion, 100%, is obtained for the catalyst containing the two metals in mass ratio Cu:Co = 2:8. Interestingly, similar catalytic performances were obtained for the same ratio in the case of catalysts based on CuNi/SBA-15 as reported in stage II/2013. These results suggest that (i) a ratio M_1: M_2 = 1:4, where M_1 = Cu and M_2 = Ni(Co) represents the optimum ratio at which the synergistic interactions between the two metals have positive effects on the physico-chemical and catalytic properties of materials and (ii) as also shown for the CuNi system, the bimetallic particles obtained by our approach are not classical alloys, but rather hetero-structures which share an mixt interface, with no segregation of copper on the surface of cobalt or nickel. For CuCo system, the results indicate similar catalytic

behaviors as CuNi system. Additional increase of the copper amount (CuCo55 and CuCo82 samples) leads to the gradual decrease in the catalytic activity. Based on data from *in-situ* XRD and TPR, it is considered that the decrease in catalytic activity is caused by the increase of copper particle size, especially for sample CuCo82. In addition, since the activity of this catalyst is similar to that of mono-metallic cobalt catalyst, it is likely that the catalytic activity is mainly attributed to cobalt. As regards the selectivity, as a general tendency, one observes a predilection of the catalysts for the hydrogenation of the C = O double bond of cinnamaldehyde However, there are no major influences of the composition and particle size on the catalytic selectivity. Thus, for sample CuCo01, the selectivity to CNOL at small conversions is around 80% and it decreases gradually up to ~ 50% with increase in conversion. Instead, for bimetallic catalysts CuCo28 and CuCo55, it can be observed a roughly constant selectivity around 50%, up to a conversion of ~ 40%, after that it suddenly decreases. This behavior can be explained by the synergistic action of copper and cobalt, the latter being responsible for the increased selectivity to CNOL (cobalt is known to be selective for CNOL due to the width of the band *d*) while it is maintained a constant value for copper. Indeed, the increasing of copper amount in the sample (CuCo82) decreases the selectivity towards 60%, but its evolution with conversion follows the trend observed for the two bimetallic samples.

(ii) Results obtained for catalytic runs at 10 bars

Conversion and selectivity curves obtained for catalytic tests carried out at a pressure of 10 bars are shown in Fig. 7.

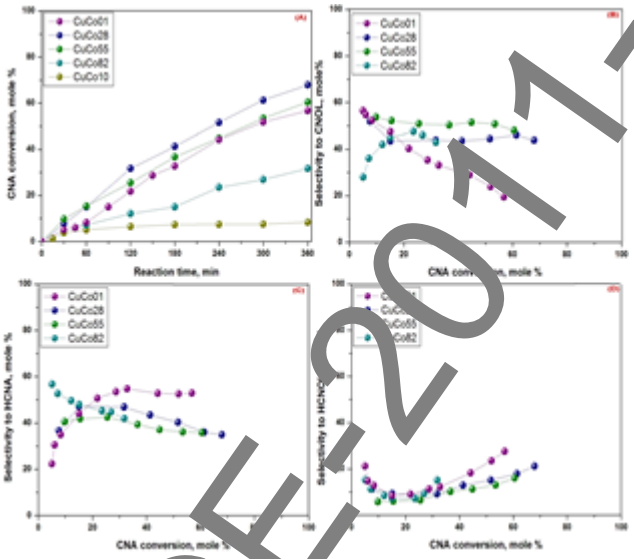

Fig. 7 Conversion of CNA as function of reaction time (A), selectivity to CNOL (B), HCNA (C) and HCNOL (D) for catalyst of CuCo/SBA-15 type. (Reaction conditions: *T_{red} = 500 °C for sample CuCo01 and 350 °C for other samples; $T_{reaction}$ = 130 °C, 0.256 g catalyst; 1 mL CNA, 40 mL isopropanol as solvent,agitation rate = 750 rpm*).

For these results one can outline three conclusions: (i) in general, as compared to the results obtained at atmospheric pressure, the catalytic activity is improved for the most samples, excepting the samples containing mono-metallic copper, (ii) the selectivity to CNOL is diminished by about 20% while the selectivity to HCNA is increased by the same percentage, and (iii) the trends for increased activity with the chemical composition and for selectivity to CNOL are maintained, irrespective of pressure. Because of the interesting properties of cobalt-based materials, a sample of Co/SBA-15 was tested in the hydrogenation reaction of furfural (product derived from biomass).[7]

***The original results of these studies have been subjects of 3 communications at international scientific events, 2 ISI-ranked articles submitted for publication[2,7] and 3 articles in preparation[8-10]* (see Annex at the report).**

References

1. Dumitriu, E; Scientific Report on the implementation of project PN-II-ID-PCE-2011-3-0868, 2012.
2. Dragoi, B, Ungureanu, A.; Ciotonea, C., Chirieac, A.; Petit, S.; Royer, S.; Dumitriu, E. *ACS Appl. Mater. Interfaces*, 2014, *submitted*.
3. Ungureanu, A.; Dragoi, B.; Chirieac, A.; Ciotonea, C.; Royer, S.; Duprez, D.; Mamede, A.S.; Dumitriu, E. *ACS Appl. Mater. Interfaces*, 2013, **5**, 3010.
4. Denise, B.; Sneeden, R.P.A.; Beguin, B.; Cherifi, O. *Appl. Catal*., 1987, **30**, 353.
5. Dandekar, A.; Vannice, M.A. *Appl. Catal B: Environ.* 1999, **22**, 179.
6. Chinchen, G.C.; Hay, C.M.; Vandevell, H.D.; Waugh, K.C., *J. Catal*. 1987, **103**, 79.
7. Audemar, M.; Ciotonea, C.; De Oliveira Vigier K.; Royer, S.; Ungureanu, A.; Dragoi, B.; Dumitriu, E.; Jérôme, F. *ChemSusChem*, 2014, *submitted*.
8. Ciotonea, C.; Mazilu, I.; Dragoi, B.; Catrinescu, C.; Dumitriu, E.; Ungureanu, A.; Alamdari, H.; Petit, S.; Royer S. *J. Am. Chem. Soc*., 2014, *in preparation*.
9. Ciotonea, C.; Dragoi, B.; Ungureanu, A.; Alamdari, H.; Petit, S.; Dumitriu, E. ; Royer, S. *Chem. Mater*., 2014, *in preparation*.
10. Mazilu, I., Ungureanu, A.; Dragoi, B.; Ciotonea, C.; Rudolf, C.; Chirieac, A.; Petit, S.; Royer, S.; Dumitriu, E. *Microporous and Mesoporus Mater*. 2014, *in preparation*.

Project leader,

Prof.dr.ing. Emil DUMITRIU